Wind speed measurements using distributed fiber optics: a wind tunnel study

Justus G.V. van Ramshorst[1,4], Miriam Coenders-Gerrits[1], Bart Schilperoort[1], Bas J.H. van de Wiel[2], Jonathan G. Izett[2], John S. Selker[3], Chad W. Higgins[3], Hubert H.G. Savenije[1], and Nick C. van de Giesen[1]

[1]Delft University of Technology, Water Resources Section, Stevinweg 1, 2628 CN Delft, The Netherlands
[2]Delft University of Technology, Geoscience and Remote Sensing, Stevinweg 1, 2628 CN Delft, The Netherlands
[3]Oregon State University, Biological and Ecological Engineering, 116 Gilmore Hall, Corvallis, Oregon 97331, USA
[4]University of Göttingen, Bioclimatology, Büsgenweg 2, 37077 Göttingen, Germany

Correspondence: Justus van Ramshorst (justus.vanramshorst@uni-goettingen.de)

Abstract. Near-surface wind speed is typically only measured by point observations. The Actively Heated Fiber-Optic (AHFO) technique, however, has the potential to provide high-resolution distributed observations of wind speeds, allowing for better characterization of fine-scale processes. Before AHFO can be widely used, its performance needs to be tested in a range of settings. In this work, experimental results on this novel observational wind-probing technique are presented. We utilized a

5   controlled wind-tunnel setup to assess both the accuracy and the precision of AHFO under a range of operational conditions. The technique allows for wind speed characterization with a spatial resolution of 0.3 m on a 1 s time scale. The flow in the wind tunnel was varied in a controlled manner, such that the mean wind, ranged between 1 and 17 ms^{-1}. The AHFO measurements are compared to sonic anemometer measurements and show a high overall correlation (0.85-0.98). Both the precision and accuracy of the AHFO measurements were also greater than 95%. We conclude that the AHFO has potential to be employed as

10   an outdoor observational technique. It allows for characterization of spatially varying fields of mean wind in complex terrain, such as in canopy flows or in sloping terrain. In the future, the technique could be combined with conventional Distributed Temperature Sensing (DTS) for turbulent heat flux estimation in micrometeorological/hydrological applications.

1 Introduction

15   This work presents the results of a wind tunnel study designed to test the novel Active Heated Fiber-Optic (AHFO) (Sayde et al. (2015)) wind speed measurement technique in controlled airflow conditions. The primary aims of the experiment were to assess the directional sensitivity and signal-to-noise ratio of AHFO.

Wind speed is most commonly observed using in-situ point measurement techniques. As a result, the spatial distribution of field observations is limited. While it is possible to obtain distributed wind speed observations with remote sensing (e.g.,Goodberlet et al. (1989)), the spatial resolution is too low for many micrometeorological applications.

Many field experiments assume Taylor's frozen flow hypothesis (Taylor (1938)) in order to estimate fluxes with similarity
5   theory (e.g.,Higgins et al. (2009); Kelly et al. (2009); Bou-Zeid et al. (2010); Patton et al. (2011)). However, similarity theory only holds for idealized homogeneous/stationary conditions, which are rarely met in practice, resulting in a model containing strong assumptions, which often leads to significant errors (Ha et al. (2007); Higgins et al. (2012); Thomas et al. (2012)). In real, non-idealized situations, even slight surface heterogeneities can lead to dramatic impacts on the spatial structure of the flow in the surface boundary layer. Further, even if perfect surface homogeneity was possible, other atmospheric (surface)
10   conditions are often nonstationary as well (Holtslag et al. (2013)).

In the past decade, a new way to obtain spatial distributed measurements was introduced into environmental studies. High-resolution measurements could be used to check underlying assumptions and would reduce the need for such assumptions in real-world cases. Distributed Temperature Sensing (DTS) technology measures temperature at high temporal and spatial resolution over distances of up to several kilometers by using Fiber Optic (FO) cables as sensors (Selker et al. (2006a); Selker
15   et al. (2006b); Tyler et al. (2009)). High-end DTS can measure the temperature at a 1 s and 0.3 m resolution (Sayde et al. (2014)). The ability to report temperature at such high resolution has proven useful in many environmental studies (Selker et al. (2006a); Selker et al. (2006b); Tyler et al. (2008); Tyler et al. (2009); Steele-Dunne et al. (2010)), including atmospheric experiments (Keller et al. (2011); Petrides et al. (2011); Schilperoort et al. (2018); Higgins et al. (2018)); Izett et al. (2018). It has also been shown that it is possible to observe air temperature and thermal structure of near-surface turbulence with DTS
20   (Thomas et al. (2012); Euser et al. (2014); Zeeman et al. (2015), Jong et al. (2015)).

Recently, Sayde et al. (2015), introduced the AHFO technique as a means of performing independent explicit wind speed measurements using distributed temperature sensing (DTS) technology. The underlying concept of the proposed method is similar to that of a hotwire anemometer; however, instead of single point measurements, AFHO enables distributed measurements to be made at high spatial resolution. Instead of only passively measuring the temperature in the fiber (as is done with
25   DTS), one segment of the cable is actively heated. The heated segment is positioned parallel to the unheated reference segment, with a small separation, in our case 0.1 m. The temperature difference between the heated and reference segment is measured, i.e., the heated fiber and the air temperature. The temperature difference between the cables depends on the energy input as well as on the wind speed of the ambient air, which determines the magnitude of the lateral heat exchange, through advection of cooler ambient air. By setting up an energy balance for the heated cable, one can estimate the magnitude of this advective
30   heat transport, which leads to an estimate of the wind speed.

Results from a field study by Sayde et al. (2015) demonstrated promising performance of the AHFO technique, but they recommended further tests be performed in controlled airflow conditions. First, the heat transfer model assumes the flow is normal to the axis of the fiber. Sayde et al. (2015) developed a first-order estimate of the influence of a non-normal angle of attack (the difference between the wind direction and the axis of the fiber), using a directional sensitivity equation from
35   hotwire anemometry (Webster (1962); Hinze (1975);Perry (1982);Adrian et al. (1984)), but it needs to be tested in a controlled

setting to determine its validity. Second, Sayde et al. (2015) highlight the importance of a sufficient signal-to-noise ratio when conducting measurements. They show that the temperature difference between the heated and reference segments gives a good estimate for this ratio. The influence of the directional sensitivity and the signal-to-noise ratio on the measurement accuracy and precision is investigated and the results are used to propose a method to estimate the precision for future experiments with

5   AHFO, hence our work will improve the possibilities for successful application of AHFO in future field experiments.

An overview of the experimental setup is presented in section 2, with the accuracy and precision of the AHFO experiments presented in section 3. In section 4, a method for estimating the precision for future experiments is introduced, followed by a short note on future studies.

2   Experimental Set-Up and Methods

10   ### 2.1   Wind tunnel experiments

We conducted a series of experiments under tightly controlled airflow conditions to improve the applicability of AHFO in experimental (field) research and to study the directional sensitivity and influence of the signal-to-noise ratio. The experiments presented were performed in a wind tunnel at Oregon State University. This wind tunnel has a closed circuit, which means the air inside is recycled. The test section of the wind tunnel has a cross-section (height by width) of 1.23 by 1.52 m, and an

15   undisturbed horizontal section of roughly 5 to 6 m which may be used for probing. During the experiment two segments of one cable (which encloses the FOs) were placed 8 cm apart: one heated and one reference segment. For validation, an independent sonic anemometer was placed approximately 0.2 m downwind of the fibers, which measures the wind speed in 3 directions. All equipment was mounted using custom-designed support material.

The angle of the fiber related to the flow, wind speed and heating rate were systematically changed. An electrical current (I)

20   is passed through the heated cable, to create the temperature difference (ΔT, e.g., 2 °C) needed to determine wind speed. By fixing the current through the stainless steel casing of the cable, the entire FO cable is heated because of the electrical resistance (R) of the stainless steel casing. The magnitude of the current needed to create a given temperature difference is dependent on the cable resistance and the wind speed, therefore the current is adjusted for each individual experiment. The amount of power applied per meter of cable, P_s (Wm^{-1}), necessary to heat the cable and to create a temperature difference, is referred to as the

25   heating rate.

The cable was mounted at four different angles in the wind tunnel, resulting in different angles of attack, in order to gain more insights into directional sensitivity. In Figure 1b the 90° set-up is visible, however the cable was also mounted at a 45°, 30° and 15° angle, with respect to the floor of the wind tunnel (see: Figure 1a, inset). During all set-ups, the lower part of the FO cable was fixed to the opening in the bottom of the wind tunnel, while the upper end was attached to an extruded aluminum

30   bar that was moved over the fixed horizontal bars, to achieve the desired cable angles. To test the performance for a range of wind speeds, ten different wind speeds were tested at every angle: 1, 3, 5, 7, 9, 11, 13, 15, 16 and 17 ms^{-1} (e.g., 4x10 = 40 setups). The AHFO wind speed measurements can be calibrated by comparing the AHFO wind speed to a reference sonic anemometer. The wind speed in the wind tunnel was fixed at a constant value to create a steady state flow. In field experiments
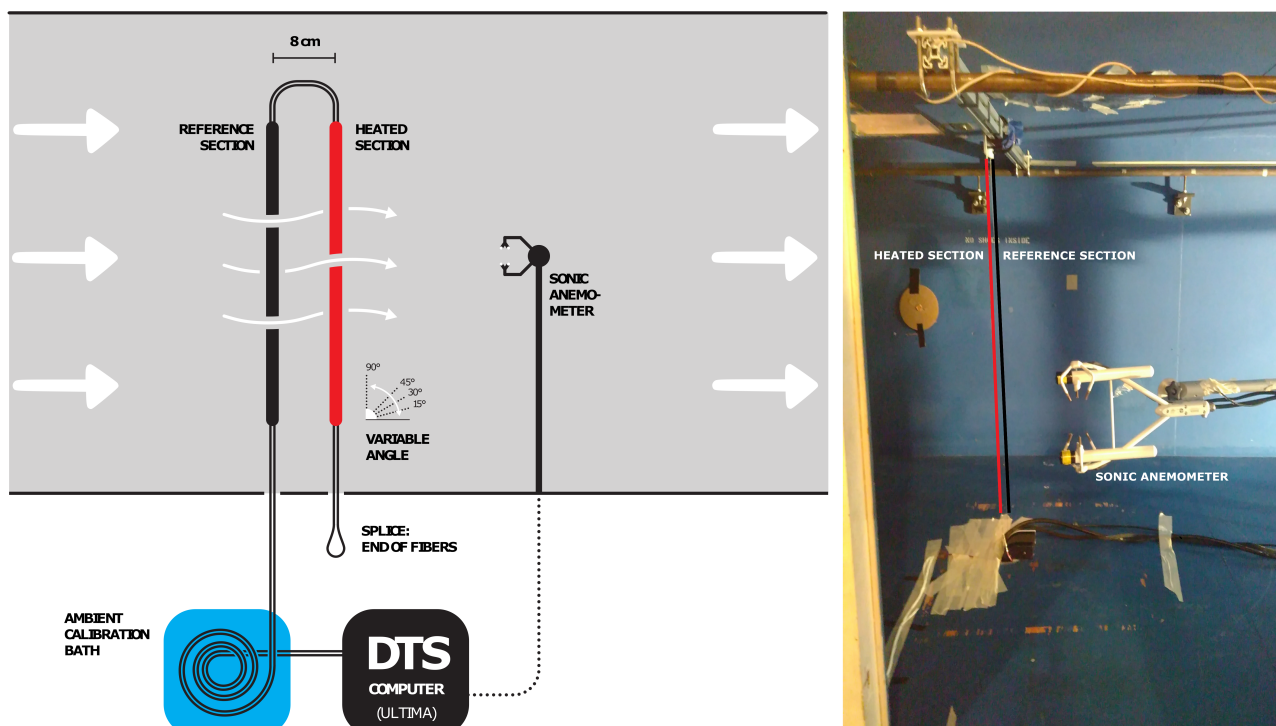
Figure 1. a) Schematic of the wind tunnel setup and b) photograph of the experimental setup in the wind tunnel.

the wind speed will vary, and the temperature difference will fluctuate accordingly if the current is fixed. For all angles and every wind speed, three temperature differences were applied in order to quantify the importance of the signal-to-noise ratio. The current was fixed to create a temperature difference (ΔT) of 2, 4 and 6 °C between the heated and reference cable. In total, 120 (4 x 10 x 3) trials were conducted with the different parameters, each with a minimum duration of 10 minutes.

5   The cable mounted in the wind tunnel consisted of a 1.34 mm outer diameter stainless steel casing that enclosed four multi-mode FOs with a diameter of 250 μm (Figure 2). Only two FOs were used and these were spliced at the end of the cable to create a duplexed FO, which results in double measurements (Hausner et al., 2011). The FOs were connected to a Silixa Ultima DTS machine (Ultima S, 2 km range, Silixa, London, UK) outside the wind tunnel.

One cable segment was heated. The stainless steel casing was connected to a power controller (MicroFUSION uF1HXTA0-

10 32-P1000-F040) by 12 AWG cables (3.31 mm^2), to heat the cable in a controlled way. Heating rates varying from 0.5-10 Wm^{-1} were used to create temperature differences to a fixed level, either 2, 4 and 6 °C, depending on the setup. The electrical resistance per meter of stainless steel casing (R_s) is 1.67 (Ωm^{-1}) and is constant along the length. For the length of a cable segment (B, (m)), $R = R_s B$, where R (Ω) is the total resistance of a cable segment. The same holds for $P = P_s B$, where P (W) is the total power input for a cable segment. The heating rate for a cable segment (Wm^{-1}) was controlled by fixing the
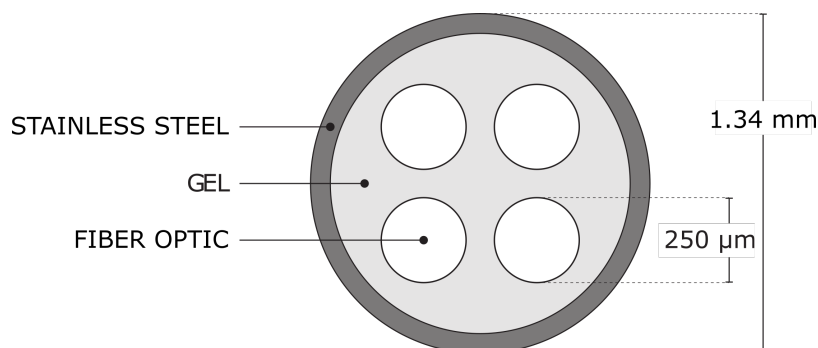
Figure 2. Cross-section of the FO cable

current, I (A), during experiments, as the current is also constant over the entire heated segment, the heating rate is as well. Hence, the known relation $P = I^2 R$ (W), or in this specific case the heating rate is $P_s = I^2 R_s$ (Wm^{-1}) per meter of cable segment.

For calibration and validation of the DTS data, approximately 6 m of the FO cables was placed in a well-mixed ambient bath
5 to calibrate the DTS temperature according to the method described by Hausner et al. (2011). The temperature was verified with one probe (RBRsolo^2 T, RBR Ltd., Ottawa, Ontario, Canada). A circulating aquarium pump was placed inside the bath, to prevent stratification.

Temperatures along the FOs were sampled at 0.125 m resolution with a sampling rate of 1 Hz. The FOs were deployed in a double-ended configuration, however the data was acquired and treated as two separated single-ended channels of data. Splices
10 between ends of fiber optic cables are known to create an additional loss in signal, i.e., local higher attenuation (Tyler et al. (2009); van de Giesen et al. (2012)), this loss is normally independent of the direction. However, in processing of the raw DTS data it was found that the loss over the splice was not the same in both directions. Due to this asymmetrical structure of the splice loss, only the data of one channel was used to ensure the quality of the results, as this channel showed a regular splice loss.

15 To be able to test the accuracy of the DTS wind speed measurements independently, wind speed was sampled at 10 Hz using a sonic anemometer (IRGASON+EC100 and CR3000, Campbell Scientific, Logan, UT,USA). The sonic anemometer was mounted approximately 0.2 m behind the fiber optic cables, in the middle of the wind tunnel. As the FOs are very thin, it is assumed that these do not significantly disturb the measurement of the sonic volume (particularly at larger averaging times).

2.2 Determination of Wind Speed

20 ### 2.2.1 Determination of Wind Speed

An energy balance is used to quantify the advective energy transport from the heated cable, and therefore estimate the wind speed with DTS. The advective cooling can be converted to wind speed, because it is a function of wind speed and the

temperature difference between the heated and unheated segments. The full energy balance (in W) for a cable segment volume of length, B, is given by Sayde et al. (2015), and schematically shown in Figure 3:

$$c_s \rho_v V \frac{dT_s}{dt} = P_s B + (\bar{S}_b + \bar{S}_d + \alpha_s \bar{S}_t)(1 - \alpha_f)2r\pi B + (\bar{L}_\downarrow + \bar{L}_\uparrow)\epsilon 2r\pi B - \epsilon\sigma T_s^4 2r\pi B - h(T_s - T_f)2r\pi B \tag{1}$$
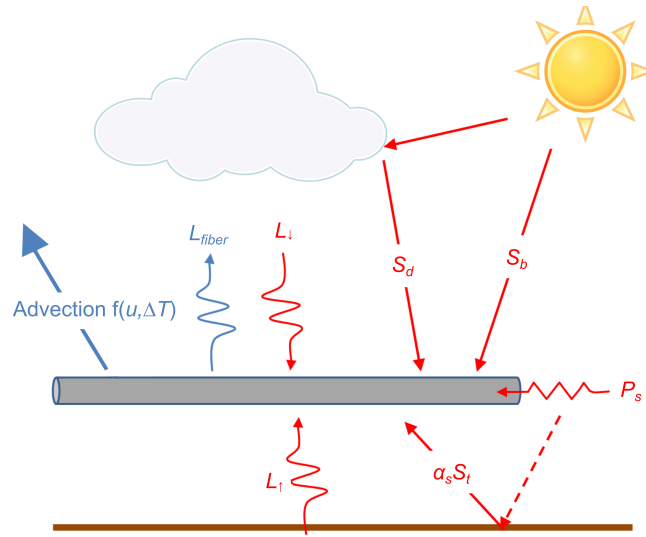
Figure 3. Schematization of the energy balance, based on Sayde et al. (2015)

Where, r is the radius of the cable ($6.7 \cdot 10^{-4}$ m in our setup); V is the volume of the cable segment ($\pi r^2 B$, in m^3), c_s is the specific heat capacity of the FO cable (502 Jkg^{-1}K^{-1}) and ρ_v is the FO cable density (800 kgm^{-3}). P_s is the heating rate per meter of cable (in Wm^{-1}); and B is the length of a cable segment (in m). $\bar{S}_b, \bar{S}_d$ and $\alpha_s\bar{S}_t$ (in Wm^{-2}) are the mean direct, diffuse and reflected short wave radiation fluxes, respectively, with α_s being the surface albedo of the ground; and α_f is the FO cable optic surface albedo. $\bar{L}_\downarrow + \bar{L}_\uparrow$ (in Wm^{-2}) are the average downward and upward longwave radiation fluxes, respectively; and ϵ is the FO cable surface emissivity. Based on the kind of stainless steel, emissivity values can range from 0.3 to 0.7 (Baldwin and Lovell-Smith (1992)); however, we assume a value of 0.5 (Madhusudana (2000)). σ is the Stefan-Boltzmann constant, $5.67 \cdot 10^{-8}$ (Wm^{-2} K^{-4}); and $\epsilon\sigma T_s^4$ is the outgoing longwave radiation of the fiber, i.e., L_{fiber}; T_s and T_f are the temperature (in K) of the heated cable segment and (unheated) reference segment (i.e., air temperature), respectively. Finally, h is the advective heat transfer coefficient (in Wm^{-2}K^{-1}). By means of the dimensionless Nusselt (Nu), Prandtl (Pr), and Reynolds (Re) numbers, h can be expressed as function of the wind speed, $h = f(u_n)$. Nu, is the ratio between the advective and conductive heat transfer, where the Nusselt number can be written as follows, (Žukauskas (1972)):

$$\text{Nu} = \frac{h d_s}{K_a} \tag{2}$$

with,

$$\mathrm{Nu} = C\mathrm{Re}^m\mathrm{Pr}^n\left(\frac{\mathrm{Pr}}{\mathrm{Pr}_s}\right)^{\frac{1}{4}} \tag{3}$$

$$\mathrm{Re} = \frac{u_n d_s}{v_a} \tag{4}$$

d_s is the fibers characteristic length ($2r$); K_a is the thermal conductivity of air and v_a the kinematic viscosity of air, respectively 0.0255 Wm^{-1}K^{-1} and 1.5 x 10^{-5} m^{2}s^{-1} (Tsilingiris (2008)). K_a and v_a are assumed to be constant, due to the controlled conditions in the wind tunnel, but in field experiments this should be included as a variable, as K_a and v_a are temperature and relative humidity depend (Tsilingiris (2008)). C, m and n are empirical constants related to forced advection of heat by air movement. In Sayde et al. (2015), C, m and n values of 0.51, 0.5 and 0.37 are set, based on (Žukauskas (1972)). Pr is the Prandtl number and can be seen as the ratio between kinematic viscosity and thermal diffusivity, which, we assume Pr to be constant (0.72) for our range of temperatures (12-35 °C), as in Tsilingiris (2008), with Pr$_s$ (the Prandtl number for the heated fiber segment), assumed to be the same as Pr, due to the small temperature differences (max. 6 °C). Lastly, Re is the Reynolds number which is used to determine the flow regime of the air along the fiber segments, i.e., Re expresses if the flow regime is laminar or turbulent. Combining Eq. 2-4 yields:

$$h = Cd^{m-1}\mathrm{Pr}^n\left(\frac{\mathrm{Pr}}{\mathrm{Pr}_s}\right)^{\frac{1}{4}} K_a v_a^{-m} u_n^m \tag{5}$$

The determination of the Nusselt number (Eq. 3) is only valid in the following ranges of Re (40-1000) and Pr (0.7-500). Re can be a limitation for higher wind speeds, especially when the diameter of the fiber is large, in our case wind speeds higher than approximately 11 ms^{-1} would be out of range. In the derivation of the energy balance (1), there is assumed to be no free convection, induced by heating of the air close to the cable, and no conduction of heat in the axial direction of the FO cable. It is also assumed there is no radiative exchange between objects close and parallel to the heated fiber, i.e., dispersion of heat from the heated cable to the reference cable is assumed to be negligible. Furthermore, a flow directed normal to the axis of FO cable is assumed by the proposed energy balance, i.e., for flow directed in a different angle, compensation is necessary to accurately estimate the wind speed.

Finally, the energy balance is simplified, by dividing Eq. 1 by $2r\pi B$, which is equal to the surface area of the FO cable. The energy balance now no longer depends on B, meaning the length of FO segment does not need to be defined. The proposed final energy balance by Sayde et al. (2015) is as follows and in Wm^{-2}:

$$\frac{c_s \rho r}{2}\frac{\mathrm{d}T_s}{\mathrm{d}t} = \frac{P_s}{2\pi r} + (\bar{S}_b + \bar{S}_d + \alpha_s \bar{S}_t)(1-\alpha_f) + (\bar{L}_\downarrow + \bar{L}_\uparrow)\epsilon - \epsilon\sigma T_s^4 - h(T_s - T_f) \tag{6}$$

where, ρ is the FO cable density per meter of cable segment: 4.5 x 10^{-3} kgm^{-1}.

2.2.2 Proposed simplified determination of Wind Speed

Due to the setup inside the wind tunnel, as opposed to outdoor conditions, some simplifications can be made. The short wave radiation can be neglected because it is an indoor experiment (no sunlight). Furthermore, we assume that there is a uniform temperature inside the wind tunnel, due to the enclosed conditions. This means the incoming radiation is dependent on the air

5   temperature, T_f. Assuming incoming $(\bar{L}_\downarrow + \bar{L}_\uparrow)$ to be black body radiation (i.e., $L_{in} = \sigma T_s^4$), the net longwave radiation loss for the fiber can be simplified accordingly by merging the incoming longwave and outgoing longwave radiation as:

$$(\bar{L}_\downarrow + \bar{L}_\uparrow)\epsilon - \epsilon\sigma T_s^4 \approx -\epsilon\sigma(T_s^4 - T_f^4) \tag{7}$$

One more additional change is made, based on our results obtained during testing of the performance of the AHFO technique. In processing of the obtained wind tunnel data it was found that by using the calculation of the Nusselt number from Žukauskas

10   (1972), Eq. 2, a $\sim 20\%$ additional bias in calculating the wind speed was created. By using a more recent version for calculating the empirical Nusselt number (Cengel and Ghajar (2014)), the bias in our study is reduced to $\sim 5\%$ Therefore, Eq. 8 is proposed to calculate the Nusselt number, where the constants C, m and n are still used; however, with the values from Table 7-1 ($C = 0.683, m = 0.466$ and $n = 1/3$) in Cengel and Ghajar (2014), rather than those in Žukauskas (1972). Next to the improved fit, the range of Re over which the equation is valid is much wider (40-4000 compared with 40-1000), and therefore

15   more applicable in future AHFO experiments.

$$\mathrm{Nu} = C\mathrm{Re}^m\mathrm{Pr}^n = 0.683\mathrm{Re}^{0.466}\mathrm{Pr}^{1/3} \tag{8}$$

Consequently, the expression of h changes as well.

$$h = Cd^{m-1}\mathrm{Pr}^n K_a \upsilon_a^{-m} u_n^m \tag{9}$$

With the long- and short-wave radiation simplifications, the simplified energy balance becomes:

20   $$\frac{c_s \rho r}{2}\frac{\mathrm{d}T_s}{\mathrm{d}t} = \frac{P_s}{2\pi r} - \epsilon\sigma(T_s^4 - T_f^4) - h(T_s - T_f) \tag{10}$$

By substituting the expression for h (Eq. 9), we can rearrange Eq. 10 to obtain an expression for wind speed. Eq. 11 will be used to estimate the wind speed in our wind tunnel study.

$$u_N = \left(\frac{0.5 P_s \pi^{-1} r^{-1} - \epsilon\sigma(T_s^4 - T_f^4) - 0.5 c_p \rho r \frac{\mathrm{d}T_s}{\mathrm{d}t}}{Cd^{m-1}\mathrm{Pr}^n K_a \upsilon_a^{-m}(T_s - T_f)}\right)^{1/m} \tag{11}$$

2.3 Directional Sensitivity analysis

Equation 11 is derived for flows normal to axis of the cable (as in Figure 1b). However, in reality the wind will not always have a 90° angle compared to the axis of the cable, especially in outside atmospheric experiments. For angles smaller than 90° the wind speed will be underestimated, as the advective heat transfer is less efficient. To be able to still determine the wind

5   speed for all angles of attack, Sayde et al. (2015) adjusted the wind speed obtained in Eq. 11 using a geometric correction from hotwire anemometry (e.g., Adrian et al. (1984)) to get the true wind speed (u_{DTS}):

$$u_{DTS} = \sqrt{\frac{u_N^2}{\cos^2(\varphi - 90°) + k^2 \sin^2(\varphi - 90°)}} \tag{12}$$

k is the directional sensitivity and φ is the angle of attack of the wind with respect to the axis of the cable, ranging from 0° to 90°.

However, during analysis of the wind tunnel data it was found that Eq. 12 was not giving satisfying results (e.g., a 22% bias between the 90° and 15° angle). In Adrian et al. (1984) it is shown that in hotwire anemometry a variety of theoretical and empirical formulas have been proposed in the past, in order to account for directional sensitivity. Alternatively, using the formula suggested by Bruun (1971) gives more satisfying results, diminishing the bias between the 90° and 15° angle to only

15   5%. This is shown in Figure 4.
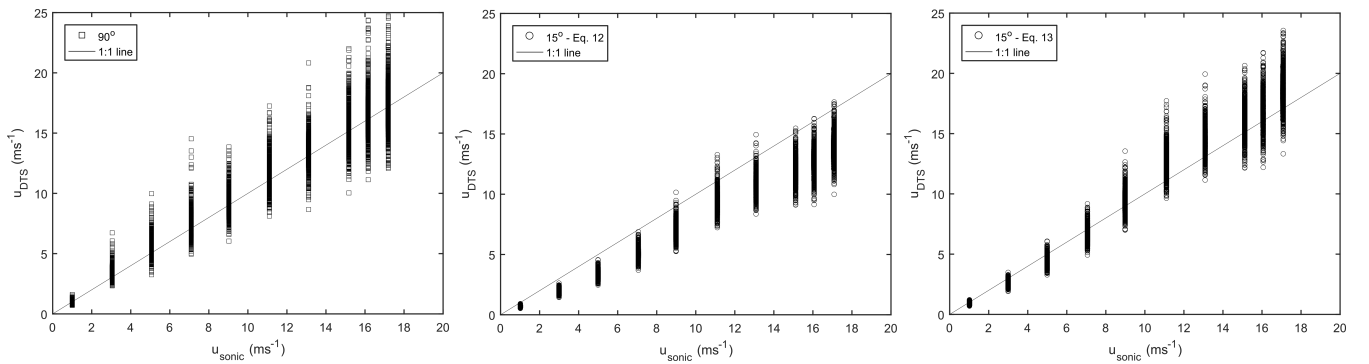
Figure 4. a) 90° angle (no correction), b) 15° angle corrected with Eq. 12., c) 15° angle corrected with Eq. 13.

Therefore, Eq. 13 is used to account for directional sensitivity in our study, with the scaling exponent, m_1, able to be optimized during calibration of the AHFO measurements. The value for m_1 obtained during calibration of our set up was 1.05.

$$u_{DTS} = \frac{u_N}{\cos(\varphi - 90°)^{m_1}} \tag{13}$$

2.4 DTS and Signal-to-Noise ratio analysis

Based on the backscattered signal of a laser pulse inside fiber optic cables, a Distributed Temperature Sensing (DTS) machine measures temperature along a complete fiber optic cable (Selker et al. (2006b)). These fiber optic cables can have lengths up to several kilometers with a spatial resolution down to 0.3 m, i.e., one DTS machine makes to thousands of near-simultaneous

5   individual measurements. Laser pulses are sent with a fixed wavelength and most backscattered light keeps this wavelength, however some backscattered laser shifts to a shorter or longer wavelength, these frequency-shifted reflections are referred to as Raman-backscatter (Selker et al. (2006a)). By counting the backscattered photons with a longer (Stokes) and shorter (Anti-Stokes) frequency, a ratio between these two can be calculated. The strength of the Anti-Stokes signal depends on temperature, hence the ratio between the power of the Stokes and Anti-Stokes changes with temperature. This principle is used to measure

10   the temperature along the cable. Consequently, a main source of noise in DTS data is white noise induced by the statistical variability in photon count from backscatter (optical shot noise). Furtherr sources of noise include Johnson-Nyquist noise.

A sufficiently high signal-to-noise ratio is essential for measurement precision with DTS. In Sayde et al. (2015) it is shown that the signal-to-noise ratio can be described as: $(T_s - T_f)/\sigma_T$. Hence the signal-to-noise ratio is related to the ΔT ($T_s - T_f$) and the measurement error of the DTS, σ_T (in this study at a 1 s sample resolution), which can be assumed constant in a lab

15   experiment. A large ΔT is obviously desirable, however, ΔT cannot be increased infinitely. The power controller can only deliver a limited amount of power to heat the fiber, which is especially relevant for the heating of long lengths of FO cable (i.e. several hundreds of meters of FO cable). Also the creation of larger temperature differences means the importance of other modes of energy transfer changes. To find realistic solutions, the effect of ΔT is investigated by using three temperature differences during the experiment. The effect of the signal-to-noise ratio is quantified, and an equation to estimate the precision

20   is presented. The precision is an indication of the variability of wind speed (e.g., RMSD), as opposed to accuracy which describes a systematic measurement error that can be removed through calibration (e.g., a bias).

3   Results

The accuracy and precision of the DTS wind speed calculations is given in Figures 5 and 6, where the velocity calculated using AHFO (calculated by Eq. 11 and 13) is compared with the velocity measured from the sonic anemometer. The temperatures

25   measured with AHFO are spatially averaged over 10 measurements (2 fibers, each with 5 measurements), i.e., this is equivalent to a height of ~ 0.9 m in the wind tunnel. Only the temperatures from the middle of the wind tunnel are used, to prevent using data with side/boundary effects. Figure 5 shows the 1 s sample rate DTS data against the 1 s average sonic anemometer data, for the four different angles of attack. Figure 6 shows the same dataset, but temporally averaged over 30 s, and for all angles. A clear improvement of the precision is visible when temporal averaging is performed. Even though the directional sensitivity

30   formula is not yet fully calibrated, the bias is negligible, with coefficients of determination ranging from 0.85-0.98. Finally, as expected, the wind speed measurement are less accurate when the wind speed angle is smaller.

To get more insight in the quality of the results, a dimensionless analysis is performed. In Figure 7, the non-dimensional wind speed accuracy for the whole wind tunnel experiment is shown. For all combinations (120 individual cases of varying
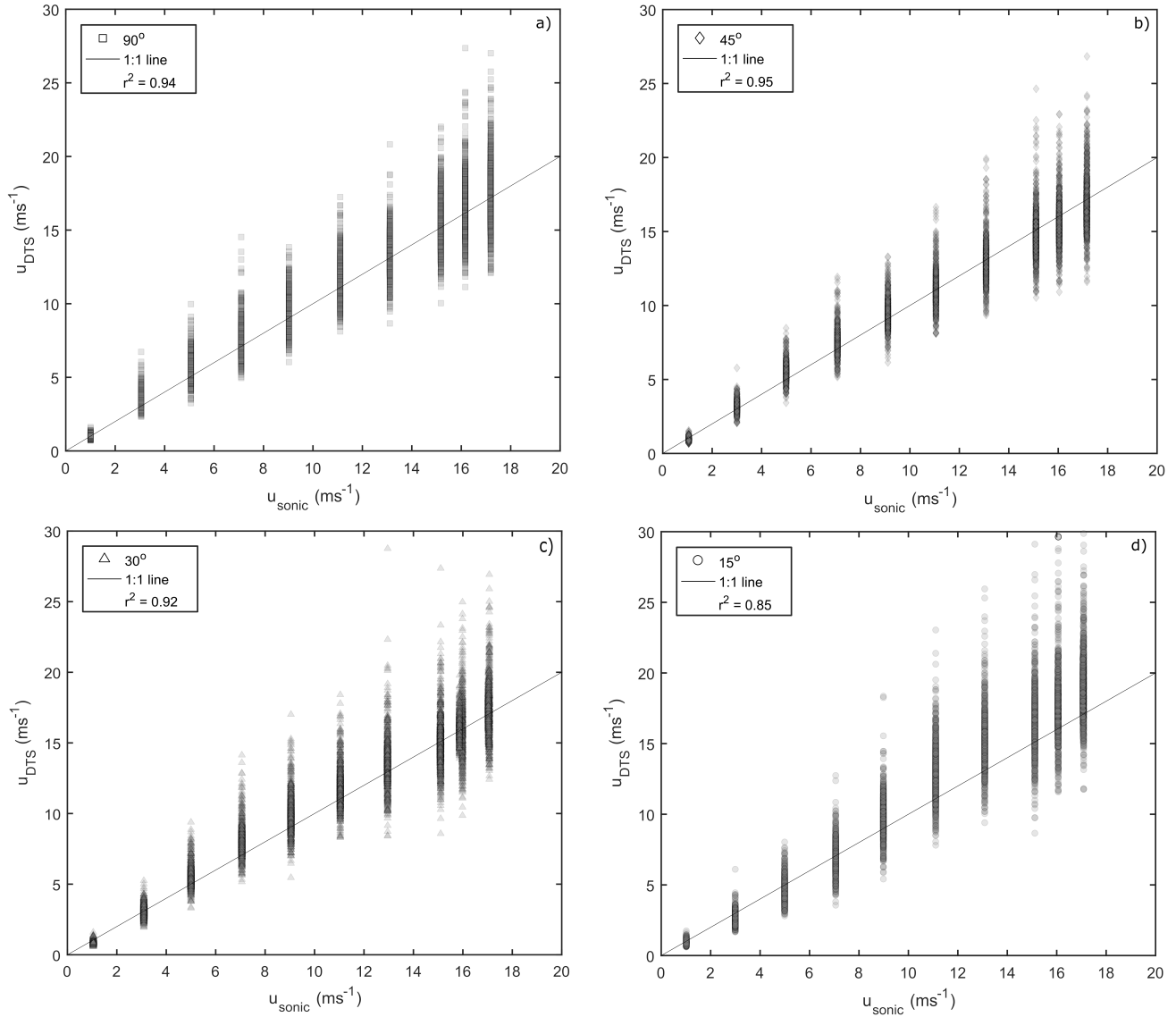
Figure 5. Comparison of AHFO and sonic anemometer wind speed at a 1 s temporal resolution, for the four different angles of attack. a) 90°, b) 45°, c) 30°, and d) 15°

wind speed, angle and ΔT), the accuracy is calculated according to Eq. 14. The accuracy is then averaged over wind speed for each ΔT and angle combination in Figure 7, indicating the size of the bias by σ_a.

$$\sigma_a = \frac{\bar{u}_{DTS} - \bar{u}_{sonic}}{\bar{u}_{sonic}} \qquad (14)$$
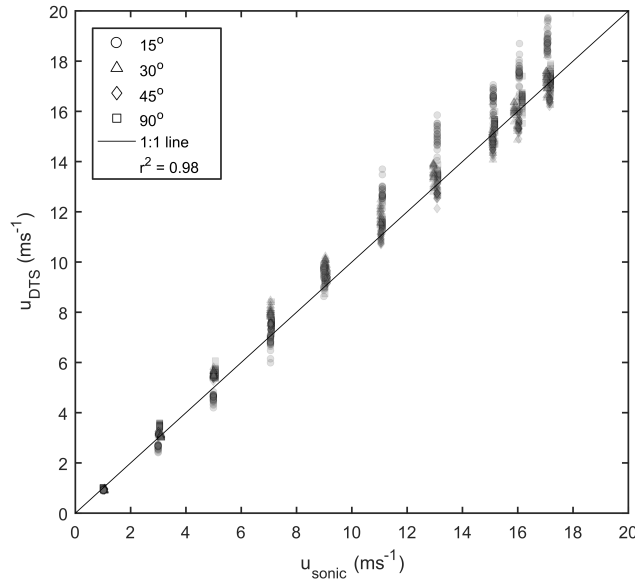
Figure 6. Comparison of AHFO and sonic anemometer wind speed averaged over 30 s for all angles of attack.

For the whole uncalibrated data set, the maximum σ_a is 5%, which is promising for future applications. The 90° angle should be the best performing angle, however it is maximal overestimating with 5%, which is probably due to neglecting small energy losses, like free convection due to heating of air close to the heated cable (Sayde et al. (2015)). With such an energy loss included, the bias of each angle will change. As a flow directed normal to the axis of FO cable is assumed by the proposed

5   energy balance, it is better to compare the other angles to the 90° angle instead of 0 bias. Doing this, it can been seen that the directional sensitivity formula is not yet optimally calibrated (e.g., the 5% difference between the 90° and 15° angle biases). This kind of error is not uncommon and in accordance with previous hotwire anemometry work, especially with small angles of attack (Adrian et al. (1984)). Nevertheless, the bias is fairly constant with increasing averaging time, which means extensive calibration can probably increase the accuracy.

10   While the accuracy (bias) remains constant over the averaging period, the relative precision, σ_p increases significantly (Fig. 8). The precision is calculated for all 120 ΔT, angle and wind speed combination, using Eq. 15. To be able to present the precision clearly, the precision is averaged over wind speed for all ΔT and angle combinations in Figure 8:

$$\sigma_p = \frac{\text{RMSD}}{\bar{u}} = \frac{\sqrt{\frac{\sum\left(\left(u_{sonic}(i) - \bar{u}_{sonic}\right) - \left(u_{DTS}(i) - \bar{u}_{DTS}\right)\right)^2}{n}}}{\bar{u}_{sonic}} \qquad (15)$$

While calculating the precision of u_{DTS}, the natural variability of the wind is excluded, by assuming the sonic anemometer

15   is able to capture this. As a result, the variability of the DTS machine u_{DTS} estimates are obtained. For each of the 120 combi-
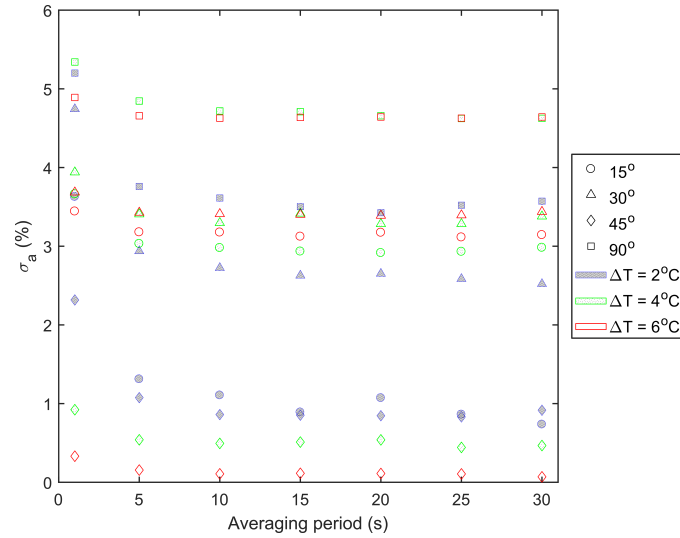
Figure 7. Bias in AHFO wind speed as a function of averaging period for different angles of attack, and different fiber heating.

nations, u_{sonic} and u_{DTS} are the average wind speeds for a given combination. $u_{sonic}(i)$ and $u_{DTS}(i)$ are single measurements during this combination.

The precision increases to a σ_p less than 5% by averaging over time. Improvement by averaging is expected due to the reduction of noise (van de Giesen et al. (2012)). As mentioned, the main source of noise in DTS data is white noise, this explains the visible improvement of the precision by $\frac{1}{\sqrt{n}}$, as signal averaging is applied, where n is the amount of measurements (Selker et al. (2006b); Kaiser and Knight (1979)).

4 Discussion

4.1 Normalized precision

In order to remove the influence of different settings (such as the choice of ΔT) and determine a general prediction of precision in future experiments, we normalize the precision. First, the precision is normalized to ΔT (Figure 9a), by multiplying by $\frac{\Delta T}{T_{error}}$. As a results, $\frac{1}{\sqrt{n}}$ dependence becomes even more clear, as shown by the black solid line showing $\frac{\gamma}{\sqrt{n}}$, where γ is σ_p at a 1 s temporal, and 10 measurement spatial, resolution. Second, the precision is also normalized to the $\frac{1}{\sqrt{n}}$ behavior, by multiplying by $\sqrt{\frac{t_{avg}}{t_{sample}}}$. Where, T_{error} and t_{sample} are given constants which depend on the performance of the DTS, in this case $T_{error} = 0.25$ K and $t_{sample} = 1$ s, according to the factory specifications. It appears that the precision can be condensed in a number, 1.6, which we denote by the symbol C_{int} (Figure 9b). Intermediate constant C_{int} can be defined as, Eq. 16:

$$C_{int} = \gamma \frac{\Delta T}{T_{error}} \sqrt{\frac{t_{avg}}{t_{sample}}} = 1.6 \qquad (16)$$
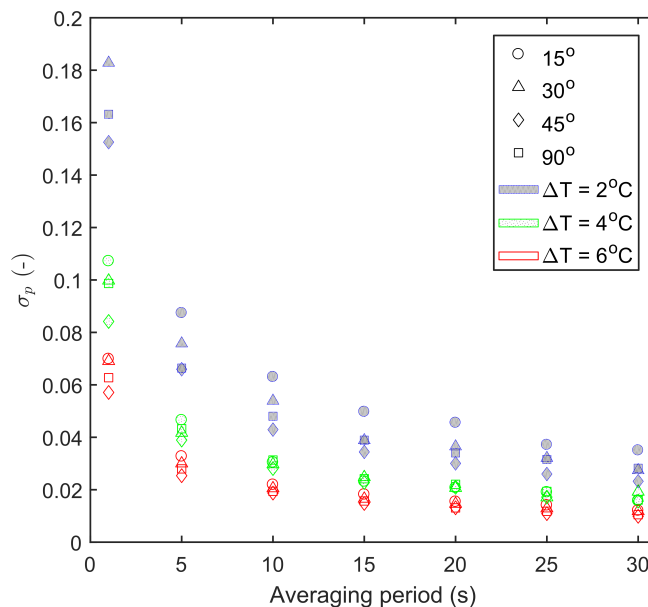
Figure 8. Precision of the AHFO wind speed measurements as a function of averaging period.
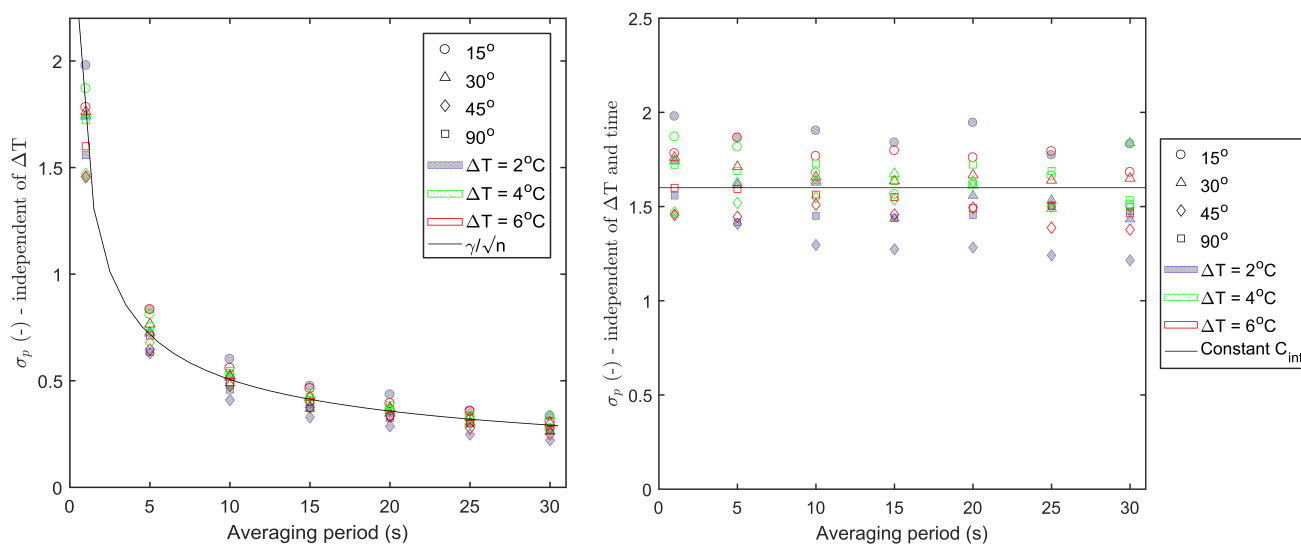
Figure 9. a) Precision of the AHFO wind speed measurements as a function of averaging period, independent of ΔT; and b) Precision of the AHFO wind speed measurements as a function of averaging period. Independent of ΔT and averaging period.

Finally, a final constant for a 1 s and 0.3 m resolution is desired, as this this is the starting point before any averaging takes place. Doing so, it is possible to increase the precision of the observation by either averaging over space or time, depending on

the scientific research question to be answered with AHFO. By using the shown $\frac{1}{\sqrt{n}}$ dependency, we can easily convert C_{int} into C_{DTS}, by multiplying C_{int} by $\sqrt{\frac{10}{1}}$, as n is 10 times less.

$$C_{DTS} = C_{int}\sqrt{10} = 1.6\sqrt{10} = 5.06 \tag{17}$$

4.2 Precision prediction

5 At the start of a new AHFO experiment it is unknown how to make sure the signal-to-noise ratio is sufficient, such that σ_p is small. However, given the result that the increase in precision behaves independent of ΔT and the averaging time, it is possible to make a prediction for the precision of future work.

In outdoor experiments, the only setting which can be changed is the heating rate, P_s, which is assumed to be fixed at a single value. The idea behind the precision prediction is to guide the choice of a heating rate, such that a preferred precision is 10 achieved for a known dominant wind speed range. As the wind speed outside will vary naturally, ΔT will change accordingly. Therefore, to obtain an expression where P_s is the only unknown, ΔT first needs to be expressed as a function of the wind speed u_n and the heating rate (P_s). This can be done by using Eq. 11. To obtain a first estimate, some assumptions can be made. The numerator of Eq. 11 consists of three terms, of which the first one with heating rate (P_s) is dominant compared to the other ones, namely 10-100 times bigger. When these minor terms are neglected Eq. 11 can be simplified to:

$$15 \quad u_N = \left(\frac{0.5 P_s \pi^{-1} r^{-1}}{C d^{m-1} \mathrm{Pr}^n K_a \upsilon_a^{-m} (T_s - T_f)} \right)^{1/m} = \left(\frac{A P_s}{B \Delta T} \right)^{1/m} \tag{18}$$

With $A = 0.5\pi^{-1}r^{-1}$, $B = C(d)^{m-1}\mathrm{Pr}^n K_a \upsilon_a^{-m}$ and $\Delta T = T_s - T_f$, resulting in an expression for ΔT as a function of wind speed:

$$\Delta T = \frac{A P_s}{B u_n^m} \tag{19}$$

Knowing this expression of ΔT, Eq. 19 can again be rewritten into Eq. 20, which expresses the precision estimate, with P_s 20 as only parameter which can be changed during an experiment.

$$\sigma_p = C_{DTS} \frac{B T_{error} u_n^m}{A P_s} \sqrt{\frac{1}{n}} \tag{20}$$

Where n is the number of measurements over which the observed wind speed is averaged, in either space or time domain. By assuming that all constants are known from literature and the set-up, a first estimate of the error can be made for every velocity or heating rate given. If a dominant wind speed range for a new project is known, an associated heating rate can be 25 found, such that the error is sufficiently small.

As an example, Figure 10 shows the estimated precision for our experiment at 1 s and 0.675 m resolution over a range of wind speeds and heating rates. If the diameter of the fiber is different, this is taken into account via term A from Eq. 20, which includes the radius ($d = 2r$). Also, when a DTS machine with a different performance is used, this can be implemented by changing T_{error} accordingly. Of course different applications will demand different space-time averaging windows, depending on the scientific research question to be answered with AHFO, which option is included by $\sqrt{\frac{1}{n}}$.
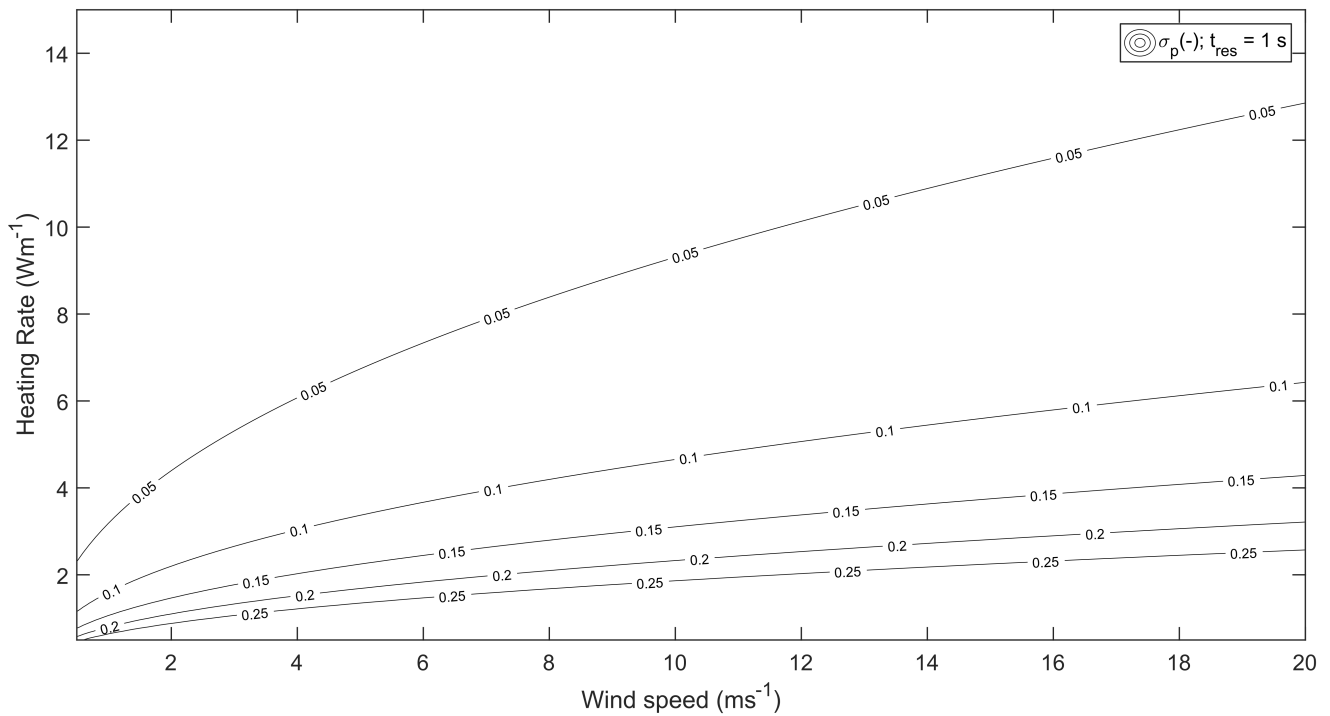
Figure 10. Expected precision (contour lines) for a given heating rate and wind speed as calculated from Eq. 20, with a 1 s temporal resolution, averaged over 10 measurements.

In outdoor experiments, the influence of the short and long wave radiation will be present. However, as long as the radiation is the same for the heated and non-heated segment, this does not influence the error estimation, as for the signal-to-noise ratio, ΔT is the most important factor. When the heated and reference fiber are close to each other, which is also needed for properly estimating the wind speed, both fibers will experience a similar contribution of external radiation, such that the overall ΔT will be relatively unaffected by this factor.

4.3 Using AHFO outdoors

The experiments described here were performed in a controlled wind tunnel environment. When performing outdoor AHFO experiments, several factors need to be considered. First of all, during field experiments the relative humidity and tempera-

ture might have such a big range that assuming certain parameters (e.g., K_a and v_a) as constant is not applicable anymore (Tsilingiris (2008)). Furthermore, for small wind speeds (e.g., $< 1 \text{ ms}^{-1}$), the neglection of energy losses like free convection seems not entirely applicable, as is visible in the strong convergence of the contour lines in Figure 10. This is confirmed in our study, where it was visible that the response is different between a well ventilated and non-ventilated cable, hence the

5 accuracy is dependent on the wind speed. Although not shown in this paper, it seemed there was no time response difference between a vertical or horizontal mounted heated cable, however by mounting the cable in a horizontal or vertical direction, free convection might influence the temperature measurements as the heated air is moving upward. It is shown that AHFO can give reliable wind speed measurements, however the precision and accuracy is not as good as with a sonic anemometer. The major addition of AHFO is the possibility to sample the wind speed with a high spatial distribution. Finally, when measuring in the

10 field, the use of high quality reference point measurements (e.g., sonic anemometer) is recommended, for example to be able to compensate for possible biases. A sonic anemometer can also be useful to determine the angle of attack, as this is not (yet) possible with one single fiber. A more complex 3D set-up is necessary to be able to do this with DTS/AHFO (Zeeman et al. (2015)).

  Despite these remarks, it will be interesting to perform outdoor tests in complex terrain, for both micrometeorological and

15 hydrological applications, as AHFO gives a lot of insights in spatial varying wind fields. AHFO can be especially interesting in non-homogenous field sites, like forests, which are already studied with other DTS applications (Schilperoort et al. (2018)). Moreover, the ability to measure spatial varying wind fields can be useful for estimating sensible heat fluxes in a variety of atmosphere-vegetation-soil continuums.

5 Conclusions

20 Through a series of controlled wind tunnel experiments, new insights into the accuracy and precision of the newly introduced AHFO wind speed measuring technique were obtained. With high spatial (0.3 m) and temporal (1 s) resolution, the AHFO wind speed measurements agreed very well with the sonic anemometer measurements, with a coefficients of determination ranging from 0.85-0.98. It is also shown that the AHFO technique has the possibility to measure with a precision and accuracy of 95%. Some additional work is needed, as there still is a small overestimation, which may be caused by neglecting some

25 energy fluxes, such as free convection due to heating of the air close the heated cable. Furthermore, it is possible to optimize the directional sensitivity compensation by extended calibration.

  The error prediction equation (Eq. 20) is an important result of this work that will aid in the design of future experiments. This design tool helps with choosing a heating rate for the actively heated fiber in order to be able to create a sufficiently high precision. Based on the prevalent wind speeds of a potential field experiment site, a first estimate of an associated sufficient

30 heating rate can be calculated. Due to the way this design tool is constructed, it can be generalized for all kinds of fibers, DTS precisions, and user preferred spatial and temporal resolutions.

  The AHFO technique can reliably measure wind speeds under a range of conditions. The combination of high spatial and temporal resolution with high precision of the technique opens possibilities for outdoor application, as the key feature of the

AHFO is the ability to measure spatial structures in the flow, over scales ranging from one meter to several kilometers. In the future, the technique could be useful for micrometeorological and hydrological applications in complex terrain, allowing for characterization of spatial varying fields of mean wind speed, such as in canopy flows or in sloping terrain.

Author contributions. Justus van Ramshorst prepared and performed the experiments, worked on analyzing the data and writing the manuscript.

5   John Selker and Chad Higgins assisted with the experiments and analyzing the data and contributed to the manuscript. Miriam Coenders-Gerrits, Bart Schilperoort, Bas van de Wiel and Jonathan Izett helped with analyzing the data and contributed to the manuscript. Huub Savenije and Nick van de Giesen contributed to the manuscript.

Competing interests. The authors declare that they have no conflict of interest.

Acknowledgements. Many thanks for the practical assistance of Cara Walter and Jim Wagner with the AHFO/DTS setup and appreciation for

10   the people of the OPEnS LAB for assisting with the assembling of parts. This project was partly funded by NWO Earth and Life Sciences, Veni project 863.15.022, The Netherlands. We are also grateful for the funding by Holland Scholarship and CTEMPs.

References

Adrian, R. J., Johnson, R. E., Jones, B. G., Merati, P., and Tung, A. T.: Aerodynamic disturbances of hot-wire probes and directional sensitivity, Journal of Physics E: Scientific Instruments, 17, 62–71, https://doi.org/10.1088/0022-3735/17/1/012, 1984.

Baldwin, A. J. and Lovell-Smith, J. E. R.: The emissivity of stainless steel in dairy plant thermal design, Journal of Food Engineering, 17, 281–289, https://doi.org/10.1016/0260-8774(92)90045-8, 1992.

Bou-Zeid, E., HIGGINS, C., HUWALD, H., MENEVEAU, C., and PARLANGE, M. B.: Field study of the dynamics and modelling of subgrid-scale turbulence in a stable atmospheric surface layer over a glacier, Journal of Fluid Mechanics, 665, 480–515, https://doi.org/10.1017/S0022112010004015, http://www.journals.cambridge.org/abstract{_}S0022112010004015, 2010.

Bruun, H. H.: Interpretation of a Hot Wire Signal Using a Universal Calibration Law., Journal of Physics E: Scientific Instruments, 4, 225–231, https://doi.org/10.1088/0022-3735/4/3/016, 1971.

Cengel, Y. and Ghajar, A.: Heat and mass transfer: fundamentals and applications, McGraw-Hill Higher Education, 2014.

Euser, T., Luxemburg, W. M. J., Everson, C. S., Mengistu, M. G., Clulow, A. D., and Bastiaanssen, W. G. M.: A new method to measure Bowen ratios using high-resolution vertical dry and wet bulb temperature profiles, Hydrology and Earth System Sciences, 18, 2021–2032, https://doi.org/10.5194/hess-18-2021-2014, 2014.

Goodberlet, M. A., Swift, C. T., and Wilkerson, J. C.: Remote sensing of ocean surface winds with the special sensor microwave/imager, Journal of Geophysical Research, 94, 14 547–14 555, https://doi.org/10.1029/JC094iC10p14547, 1989.

Ha, K.-J., Hyun, Y.-K., Oh, H.-M., Kim, K.-E., and Mahrt, L.: Evaluation of Boundary Layer Similarity Theory for Stable Conditions in CASES-99, Monthly Weather Review, 135, 3474–3483, https://doi.org/10.1175/MWR3488.1, http://journals.ametsoc.org/doi/abs/10.1175/MWR3488.1, 2007.

Hausner, M. B., Suárez, F., Glander, K. E., van de Giesen, N., Selker, J. S., and Tyler, S. W.: Calibrating single-ended fiber-optic raman spectra distributed temperature sensing data, Sensors, 11, 10 859–10 879, https://doi.org/10.3390/s111110859, 2011.

Higgins, C. W., Meneveau, C., and Parlange, M. B.: Geometric Alignments of the Subgrid-Scale Force in the Atmospheric Boundary Layer, Boundary-Layer Meteorology, 132, 1–9, https://doi.org/10.1007/s10546-009-9385-3, https://doi.org/10.1007/s10546-009-9385-3, 2009.

Higgins, C. W., Froidevaux, M., Simeonov, V., Vercauteren, N., Barry, C., and Parlange, M. B.: The Effect of Scale on the Applicability of Taylor's Frozen Turbulence Hypothesis in the Atmospheric Boundary Layer, Boundary-Layer Meteorology, 143, 379–391, https://doi.org/10.1007/s10546-012-9701-1, 2012.

Higgins, C. W., Wing, M. G., Kelley, J., Sayde, C., Burnett, J., and Holmes, H. A.: A high resolution measurement of the morning ABL transition using distributed temperature sensing and an unmanned aircraft system, Environmental Fluid Mechanics, 18, 683–693, https://doi.org/10.1007/s10652-017-9569-1, https://doi.org/10.1007/s10652-017-9569-1, 2018.

Hinze, J.: Turbulence, McGraw-Hill Higher Education, New York, 1975.

Holtslag, A. A., Svensson, G., Baas, P., Basu, S., Beare, B., Beljaars, A. C., Bosveld, F. C., Cuxart, J., Lindvall, J., Steeneveld, G. J., Tjernström, M., and Van De Wiel, B. J.: Stable atmospheric boundary layers and diurnal cycles: Challenges for weather and climate models, Bulletin of the American Meteorological Society, 94, 1691–1706, https://doi.org/10.1175/BAMS-D-11-00187.1, 2013.

Izett, J. G., Schilperoort, B., Coenders-Gerrits, A. M. J., Baas, P., Bosveld, F. C., and Van De Wiel, B. J. H.: Missed fog? On the potential of high-resolution 2 observations of shallow fog., Boundary-Layer Meteorology, IN REVIEW, 2018.

Jong, S. A. P. D., Slingerland, J. D., and Giesen, N. C. V. D.: Fiber optic distributed temperature sensing for the determination of air temperature, pp. 335–339, https://doi.org/10.5194/amt-8-335-2015, 2015.

Kaiser, R. and Knight, W.: Digital signal averaging, Journal of Magnetic Resonance (1969), 36, 215–220, https://doi.org/10.1016/0022-2364(79)90096-9, http://linkinghub.elsevier.com/retrieve/pii/0022236479900969, 1979.

Keller, C. A., Huwald, H., Vollmer, M. K., Wenger, A., Hill, M., Parlange, M. B., and Reimann, S.: Fiber optic distributed temperature sensing for the determination of the nocturnal atmospheric boundary layer height, Atmospheric Measurement Techniques, 4, 143–149, https://doi.org/10.5194/amt-4-143-2011, http://www.atmos-meas-tech.net/4/143/2011/, 2011.

Kelly, M., Wyngaard, J. C., and Sullivan, P. P.: Application of a Subfilter-Scale Flux Model over the Ocean Using OHATS Field Data, Journal of the Atmospheric Sciences, 66, 3217–3225, https://doi.org/10.1175/2009JAS2903.1, http://journals.ametsoc.org/doi/abs/10.1175/2009JAS2903.1, 2009.

Madhusudana, C.: Accuracy in thermal contact conductance experiments - the effect of heat losses to the surroundings, International Communications in Heat and Mass Transfer, 27, 877–891, https://doi.org/10.1016/S0735-1933(00)00168-8, http://linkinghub.elsevier.com/retrieve/pii/S0735193300001688, 2000.

Patton, E. G., Horst, T. W., Sullivan, P. P., Lenschow, D. H., Oncley, S. P., Brown, W. O. J., Burns, S. P., Guenther, A. B., Held, A., Karl, T., Mayor, S. D., Rizzo, L. V., Spuler, S. M., Sun, J., Turnipseed, A. A., Allwine, E. J., Edburg, S. L., Lamb, B. K., Avissar, R., Calhoun, R. J., Kleissl, J., Massman, W. J., Paw U, K. T., and Weil, J. C.: The Canopy Horizontal Array Turbulence Study, Bulletin of the American Meteorological Society, 92, 593–611, https://doi.org/10.1175/2010BAMS2614.1, http://journals.ametsoc.org/doi/abs/10.1175/2010BAMS2614.1, 2011.

Perry, A.: Hot-wire anemometry, Clarendon press, Oxford, UK, 1982.

Petrides, A. C., Huff, J., Arik, A., van de Giesen, N., Kennedy, A. M., Thomas, C. K., and Selker, J. S.: Shade estimation over streams using distributed temperature sensing, Water Resources Research, 47, https://doi.org/10.1029/2010WR009482, http://doi.wiley.com/10.1029/2010WR009482, 2011.

Sayde, C., Buelga, J. B., Rodriguez-Sinobas, L., El Khoury, L., English, M., van de Giesen, N., and Selker, J. S.: Mapping variability of soil water content and flux across 1-1000 m scales using the Actively Heated Fiber Optic method, Water Resources Research, 50, 7302–7317, https://doi.org/10.1002/2013WR014983, http://doi.wiley.com/10.1002/2013WR014983, 2014.

Sayde, C., Thomas, C. K., Wagner, J., and Selker, J.: High-resolution wind speed measurements using actively heated fiber optics, Geophysical Research Letters, 42, 10 064–10 073, https://doi.org/10.1002/2015GL066729, 2015.

Schilperoort, B., Coenders-Gerrits, M., Luxemburg, W., Jiménez Rodríguez, C., Cisneros Vaca, C., and Savenije, H.: Technical note: Using distributed temperature sensing for Bowen ratio evaporation measurements, Hydrology and Earth System Sciences, 22, 819–830, https://doi.org/10.5194/hess-22-819-2018, https://www.hydrol-earth-syst-sci.net/22/819/2018/, 2018.

Selker, J., van de Giesen, N. C., Westhoff, M., Luxemburg, W., and Parlange, M. B.: Fiber optics opens window on stream dynamics, Geophysical Research Letters, 33, 27–30, https://doi.org/10.1029/2006GL027979, 2006a.

Selker, J. S., Thévenaz, L., Huwald, H., Mallet, A., Luxemburg, W., Van De Giesen, N., Stejskal, M., Zeman, J., Westhoff, M., and Parlange, M. B.: Distributed fiber-optic temperature sensing for hydrologic systems, Water Resources Research, 42, 1–8, https://doi.org/10.1029/2006WR005326, 2006b.

Steele-Dunne, S. C., Rutten, M. M., Krzeminska, D. M., Hausner, M., Tyler, S. W., Selker, J., Bogaard, T. A., and van de Giesen, N. C.: Feasibility of soil moisture estimation using passive distributed temperature sensing, Water Resources Research, 46, https://doi.org/10.1029/2009WR008272, http://doi.wiley.com/10.1029/2009WR008272, 2010.

Taylor, G. I.: The Spectrum of Turbulence, Proceedings of the Royal Society A: Mathematical, Physical and Engineering Sciences, 164, 476–490, https://doi.org/10.1098/rspa.1938.0032, http://rspa.royalsocietypublishing.org/cgi/doi/10.1098/rspa.1938.0032, 1938.

Thomas, C. K., Kennedy, A. M., Selker, J. S., Moretti, A., Schroth, M. H., Smoot, A. R., Tufillaro, N. B., and Zeeman, M. J.: High-Resolution Fibre-Optic Temperature Sensing: A New Tool to Study the Two-Dimensional Structure of Atmospheric Surface-Layer Flow, Boundary-Layer Meteorology, 142, 177–192, https://doi.org/10.1007/s10546-011-9672-7, 2012.

Tsilingiris, P.: Thermophysical and transport properties of humid air at temperature range between 0 and 100°C, Energy Conversion and Management, 49, 1098–1110, https://doi.org/10.1016/j.enconman.2007.09.015, http://linkinghub.elsevier.com/retrieve/pii/S0196890407003329, 2008.

Tyler, S. W., Burak, S. A., McNamara, J. P., Lamontagne, A., Selker, J. S., and Dozier, J.: Spatially distributed temperatures at the base of two mountain snowpacks measured with fiber-optic sensors, Journal of Glaciology, 54, 673–679, https://doi.org/10.3189/002214308786570827, https://www.cambridge.org/core/product/identifier/S0022143000208770/type/journal{_}article, 2008.

Tyler, S. W., Selker, J. S., Hausner, M. B., Hatch, C. E., Torgersen, T., Thodal, C. E., and Schladow, S. G.: Environmental temperature sensing using Raman spectra DTS fiber-optic methods, Water Resources Research, 45, 1–11, https://doi.org/10.1029/2008WR007052, http://doi.wiley.com/10.1029/2008WR007052, 2009.

van de Giesen, N., Steele-Dunne, S. C., Jansen, J., Hoes, O., Hausner, M. B., Tyler, S., and Selker, J.: Double-ended calibration of fiber-optic raman spectra distributed temperature sensing data, Sensors (Switzerland), 12, 5471–5485, https://doi.org/10.3390/s120505471, 2012.

Webster, C. A. G.: A note on the sensitivity to yaw of a hot-wire anemometer, Journal of Fluid Mechanics, 13, 307, https://doi.org/10.1017/S0022112062000695, http://www.journals.cambridge.org/abstract{_}S0022112062000695, 1962.

Zeeman, M. J., Selker, J. S., and Thomas, C. K.: Near-Surface Motion in the Nocturnal, Stable Boundary Layer Observed with Fibre-Optic Distributed Temperature Sensing, Boundary-Layer Meteorology, 154, 189–205, https://doi.org/https://doi.org/10.1007/s10546-014-9972-9, 2015.

Žukauskas, A.: Heat Transfer from Tubes in Crossflow, pp. 93–160, https://doi.org/10.1016/S0065-2717(08)70038-8, http://linkinghub.elsevier.com/retrieve/pii/S0065271708700388, 1972.